THE BEAM TRANSPORT SYSTEM OF THE MICHIGAN STATE UNIVERSITY CYCLOTRON *

G. H. Mackenzie, E. Kashy, M. M. Gordon, and H. G. Blosser
Michigan State University
East Lansing, Michigan

Introduction

This paper describes the novel design features and associated ion-optical calculations of the Michigan State University cyclotron[1] beam transport and analysis system. The analysis system has been designed to provide doubly focused beams of 0.01% energy width; it is at present under construction and should be installed in spring of this year. It consists principally of two n = 0 circular bending magnets, each bending 45°, combined with two quadrupole lenses to give vertical focusing such that $\nu_z = 2\nu_r$. When both magnets have the same polarity an energy dispersion of 0.03%/mm is achieved; if the field in the second magnet is reversed low dispersion high intensity beams are available. The use of circular bending magnets offers considerable flexibility in the choice of beam lines, and beams can be delivered at any of seven target positions solely by changes in the excitation of the ion-optical elements; this feature will facilitate future computer control. Both linear and non-linear calculations have been made on the analysis system, and since $\nu_z = 2\nu_r$ second order aberrations in the median plane can be corrected by a sextupole placed at the intermediate vertical focus. Second order aberrations in the vertical motion are compensated by a second sextupole placed after the final quadrupole.

Layout of the Transport System

The layout is shown in Figure 1. The beam is extracted from the cyclotron via an electrostatic deflector and magnetic channel and is focused onto the slit S1 by means of four quadrupole lenses. In the high dispersion case the system (see Figure 2) forms an image of S1 at S2; beams of lower dispersion are available at C, D, and C', and a straight-through beam line is shown to the beta spectrometer and neutron facility at A and B. To first order the beam enters and leaves the bending magnets perpendicularly and vertical focusing is accomplished by means of the quadrupoles Q1 and Q2 placed 26.375 in. from the centers of the bending magnets M1 and M2. The bending magnets are separated by 60.75 in. The two sextupoles proposed are shown at SX1 and SX2. The beam analysis is essentially complete at S2, and the elements between S1 and S2 are referred to as the analysis system. The radial magnification of unity and dispersion of 0.03%/mm demand that S1 and S2 be approximately 0.3 mm to achieve the required resolution.

S2 serves as an object for the switching magnet M3 which directs the beam along the four lines shown in Figure 1. The two lines to the precision scattering chamber at G and the spectrograph at I have a dispersion and magnification which can be altered over a small range and it is possible to dispersion match[2] with the spectrograph leaving the target angle as a free parameter[3].

The Ion-optical Elements

The bending magnets (weight 7 tons) have a pole tip radius of 14.375 in. and require a field of 11.9 kG. to bend a 56 MeV proton 45°; this particle has the maximum magnetic rigidity of any produced by the cyclotron. A homogenizing gap[4] of 1/16 in. is included between the pole pieces and the yoke, and the pole tip edges are shaped to approximate to magnetic equipotentials[5]. The quadrupoles are a scaled version of a carefully optimized design used at Brookhaven[6], they are 6 in. long and are never required to produce a field gradient in excess of 3kG/in. for a maximum rigidity particle. The sextupoles now in construction are 8 in. long and are designed to yield values of $\frac{\partial^2 B}{\partial R^2}$ considerably in excess of the expected maximum value of 120 G/(in.)^2.

Fields are being measured using a Rawson rotating coil fluxmeter mounted on an automated milling table, and a proton resonance probe is used for the flat portion of the bending magnet field. The field is brought to a given setting by first raising it to 13.1 kG, then lowering it to zero, and finally going to the required value. Preliminary results of hysteresis studies[7] indicate that it will be possible to reproduce energy settings to 0.006% by this means. The field integral is calculated from measurements made at several settings, and will be obtained for other energies by interpolation; we expect that the absolute energy determination will be accurate to about 0.02%.

The Linear Calculations

The linear calculations were performed using the OPTIK code of Devlin[8]. This program searches on two parameters at a time to calculate the quadrupole field strengths and positions required to achieve a specified focusing condition for a system of any number of elements. It calculates the transfer matrices for the system and shows the effects of stops as limitations on the phase space area at the source of particles. A modification by Kosaka[9] plots the path through a system of a standard set of initial rays; for an example the rays through the analysis system are shown in Figure 3. A right-handed cartesian coordinate system is used, where the Z axis is the optic axis and the Y axis is vertical. Figure 2 clearly exhibits the $\nu_z = 2\nu_r$ character of the system.

For the present case of unit magnification

the $\nu_z = 2\nu_r$ system (which is similar in character to a single magnet with n = 0·8) gives approximately twice the resolution of a $\nu_z = \nu_r$ system (corresponding to $n = \frac{1}{2}$). This system also has the advantage that it is possible to put a sextupole to correct for second order horizontal aberrations at the intermediate vertical focus, so that its effect is confined only to rays displaced in the median plane.

The Non-Linear Calculations

Field Descriptions

The code Cartax[10] was used to trace rays through analytic fields which were expanded to second order off the median plane of the bending magnet, and to the third power of the displacement from the optic axis for the other elements. The scalar magnetic potentials used were as follows:

Bending magnet

$$\Psi_B = yf(R) - \frac{y^3}{6}\left(\frac{\partial^2 f(R)}{\partial R^2}\right) \qquad (1)$$

Quadrupole

$$\Psi_Q = xyf(z) - \frac{(x^2+y^2)}{12}xy\frac{\partial^2 f(z)}{\partial z^2} \qquad (2)$$

Sextupole

$$\Psi_s = y(3x^2-y^2)f(z) \qquad (3)$$

The function f in each case describes the fringe field of that element, as seen along a radius for the bending magnet, and along a line in the median plane parallel to the optic axis but displaced from it by 1 in. in the case of quadrupole and sextupole. The bending magnet is assumed to be symmetrical about the median plane, and quadrupole and sextupole symmetry have also been assumed. Field terms arising from quadrupole symmetry and depending on the fifth power of displacement were included but their effect was found to be small and probably less important than mechanical imperfections. The fringe fields were described by Saxon-Wood functions (equation 4) as these are well-behaved in the higher derivatives.

$$\frac{B}{B_o} = \left(1+\exp\left(\frac{R-R_o}{a}\right)\right)^{-1} \qquad (4)$$

This expression is a fairly good description for the quadrupole field, but not for the recently measured bending magnet field. The analytic and measured fields for the bending magnets are shown in Figure 4.

The Results of the Calculations

Starting midway between magnets M1 and M2, in order to take advantage of the symmetry of the analysis system, the initial conditions consisted of rays moving parallel to the optic axis and displaced horizontally or diverging vertically. This enabled the conditions for a double focus to be found, and the strength of the sextupole SX1 to be adjusted to cancel second order effects in the median plane. The vertically defocusing effect of the bending magnet fringe fields necessitated a quadrupole movement of about 1.3 in. away from the bending magnet and an increase in field strength of 4.3%.

We describe the aberrations in the usual series form[11,12], where the subscripts 1 and 2 refer to object and image coordinate systems, and the primes indicate the slopes with respect to the optic axis, e.g. $y_1' = dy_1/dz_1$.

For example,

$$x_2 = (x_2/x_1)x_1 + (x_2/x_1')x_1' + \ldots\ldots (x_2/x_1^2)x_1^2 + \ldots\ldots(x_2/x_1x_1')x_1x_1'\ldots \qquad (5)$$

and similarly for x_2', y_2 and y_2'.

Early studies, those of rays started in the sextupole SX1, showed that the most important of these aberration coefficients was the $(x_2/x_1'^2)$ term, followed by the $(x_2/y_1'^2)$ term. The first arises from the circular shape of the pole pieces, and the second from the reduced median plane velocity of the ion and the effect of the fringe field. These aberrations are corrected by two sextupoles positioned at SX1 and SX2, as shown in Figure 2. The sextupoles reduce the coefficients $(x_2/x_1'^2)$ and $(x_2/y_1'^2)$ from (-1.6×10^{-2}) in./(m-rad)^2 and (7.9×10^{-4}) in./(m-rad)^2 to essentially zero. After these errors are corrected the dominant residual aberration is the third order $(x_2/x_1'^3)$. Preliminary studies indicate that this aberration can be reduced by restoring the symmetry of the system by installing a third sextupole before Q1.

Figure 5 shows the projections in the median plane, near S2, of rays corresponding to 50 MeV protons with the indicated values of x' and y' at S1 traced through an analysis system with no sextupoles. Figure 6 is a similar diagram with sextupole field strengths of 115 G/(in)^2 for SX1 and about 100 G/(in)^2 for SX2. Figure 7 shows rays projected in the vertical plane. All three figures were obtained using the Saxon-Wood analytical field shape.

At present the cubic aberration $(x_2/x_1'^3)$ of $(-2{\cdot}1 \times 10^{-4})$ in./(m rad)^3 limits the acceptance solid angle for a given resolution; however, for many experiments with light nuclei the energy spread arising from scattering kinematics makes the present horizontal angular acceptance of $\pm$ 5 m rad more than sufficient.

Conclusions

It can be seen from Figure 6 that the analysis system of Figure 2 promises beams of 0.01% energy width from a source 0.013 in. wide and with a maximum of $\pm$ 5 m rad in the horizontal and vertical planes. Preliminary emittance measure-

ments on the beam extracted from the cyclotron by the deflector-magnetic channel combination lead us to expect about 200 n A of such beam. Elimination of a 360 c/s ripple observed on the external beam will substantially increase this figure. This figure can also be increased by reducing the cubic aberration in the horizontal plane, thus allowing an increase of the horizontal phase space acceptance area, but at the cost of an increased angular spread of the beam on target.

Contrary to many conventional analysis and transport systems where tedious shimming of the iron profile is required the system described here is flexible and easily adjusted to obtain the desired focal properties and correct the aberrations. These results are achieved with a modest amount of uncomplicated hardware, all of which is being manufactured in the laboratory machine shop. The final operating parameters of the system will be determined after tracing rays through the measured fields of the elements.

We would like to acknowledge the help of many graduate and undergraduate students in this work, notably Jim Snelgrove, Mike Greenblatt and Dave Gilbert. We would also like to thank our colleagues in the department for several stimulating discussions.

*Work supported by The National Science Foundation.

References

1. H. G. Blosser and A. I. Galonsky, I.E.E.E. Trans. on Nuclear Science 13, No. 4, 466 (1966).
2. B. L. Cohen, R.S.I. 30, 415 (1959).
3. J. B. Ball, I.E.E.E. Trans. on Nuclear Science 13, No. 4, 340 (1966).
4. Due to E. M. Purcell, see H. A. Enge, Nucl. Inst. and Meth. 28, 119 (1964).
5. C. M. Braams, Nucl. Inst. and Meth. 26, 83 (1964).
6. G. T. Danby and J. W. Jackson, B.N.L. - 7700 (1963).
7. J. Snelgrove and E. Kashy; to be published.
8. T. J. Devlin, UCRL 9727 (1961).
9. K. Kosaka, Thesis, MSUCP-13 (1962).
10. T. I. Arnette and M. M. Gordon, private communication.
11. H. A. Enge, R.S.I. 35, 278 (1964).
12. K. L. Brown, R. Bebeoch and P. Bounin, R.S.I. 35, 481 (1964).

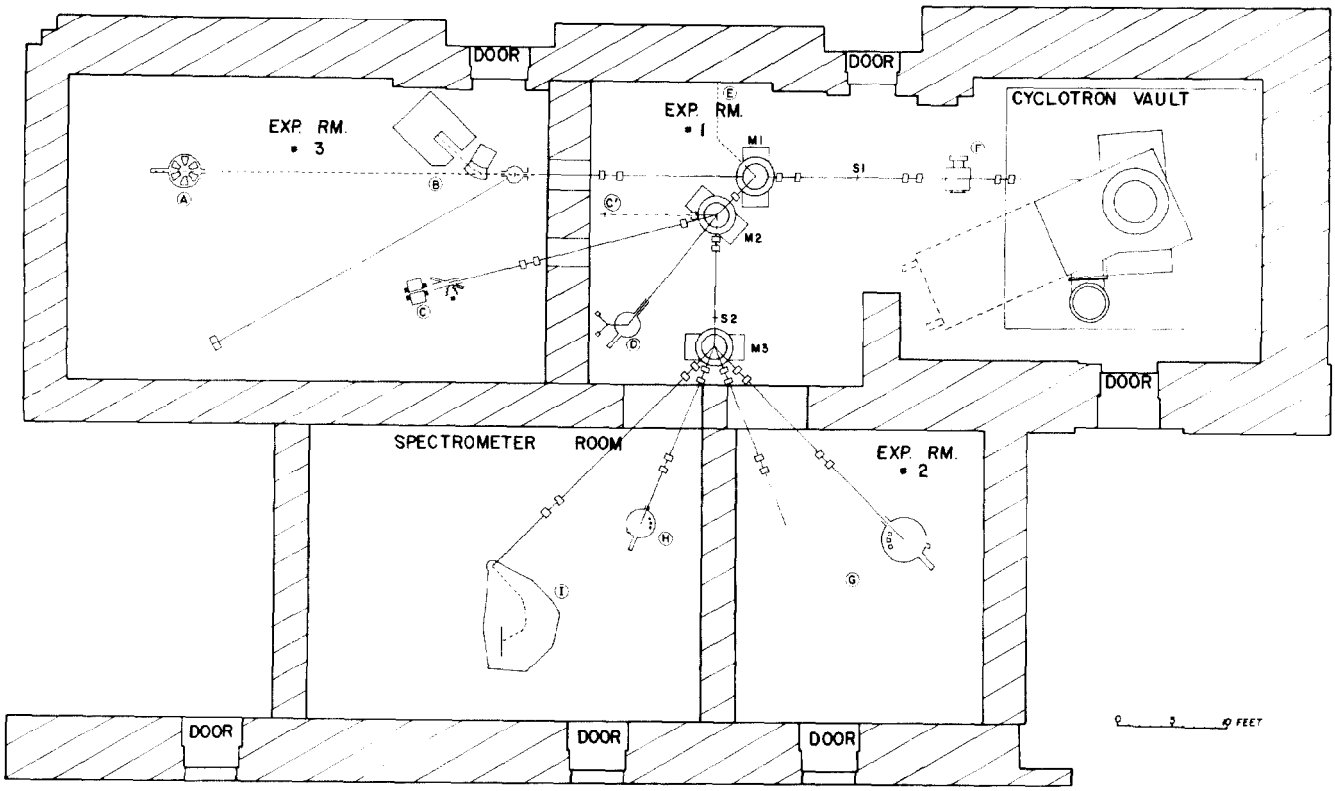

Fig. 1. The layout of the experimental areas. The items indicated in this figure are: (a) a multi-gap electron spectrometer; (b) beam stop assembly for the neutron time of flight program; (c) gamma ray facility with a bending magnet to send the beam into a well in the floor; (c') a beam of extremely small spot size to be used in biological studies; (d) polarization facility; (e) to possible future beam positions; (f) activation facility; (g) high precision scattering chamber; (h) low precision scattering chamber; (i) broad range, split pole spectrograph.

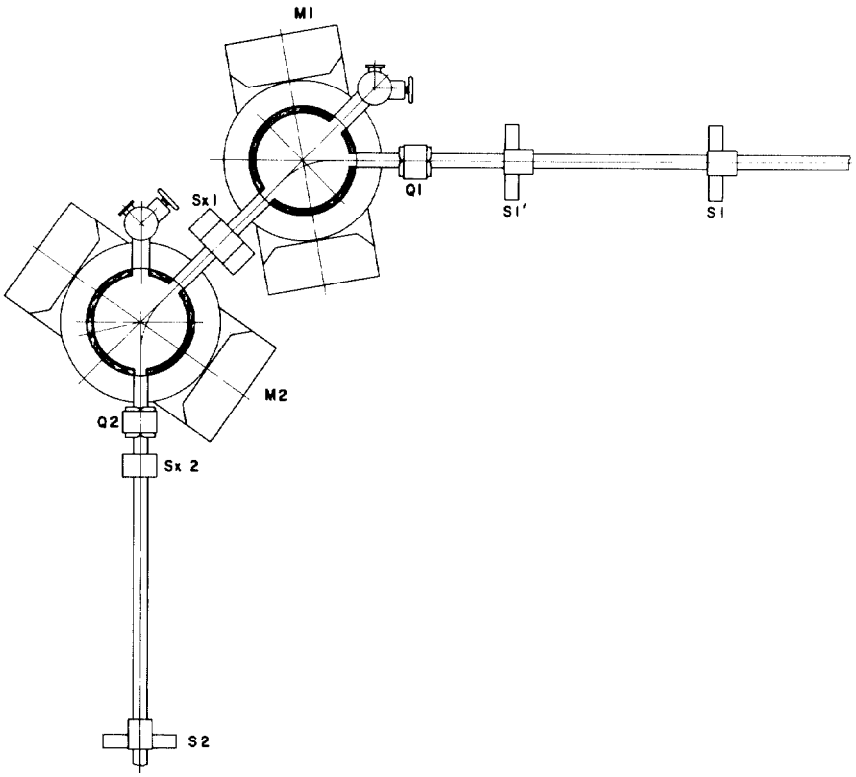

Fig. 2. The analysis system. M1 and M2 are n = 0 bending magnets, quadrupoles Q1 and Q2 provide vertical focusing, and second order aberrations are corrected by sextupoles Sx1 and Sx2. The slit S1 serves as an object for the system, the acceptance solid angle being controlled by S1', and an image is formed at slit S2.

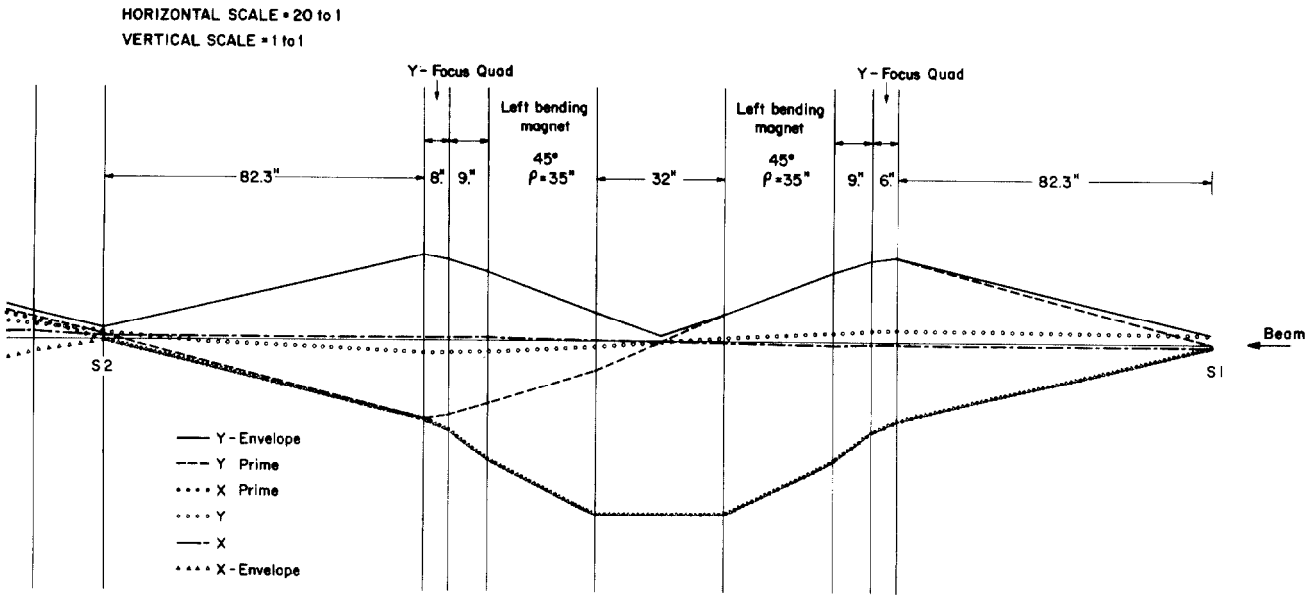

Fig. 3. The results of linear calculations on the analysis system of Figure 2. The positions of a representative set of rays are calculated at the beginning and end of each element (excluding sextupoles) and the positions joined by straight lines. Note the $\nu_z = 2\nu_r$ character of the system.

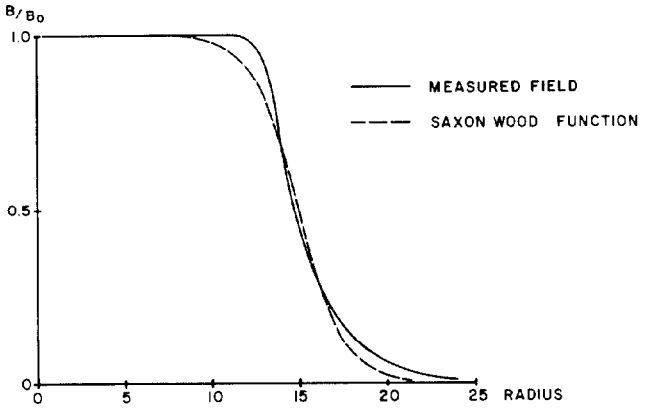

Fig. 4. A comparison of B/B_o for the recently measured bending magnet field and the Saxon-Wood form used in the non-linear calculations.

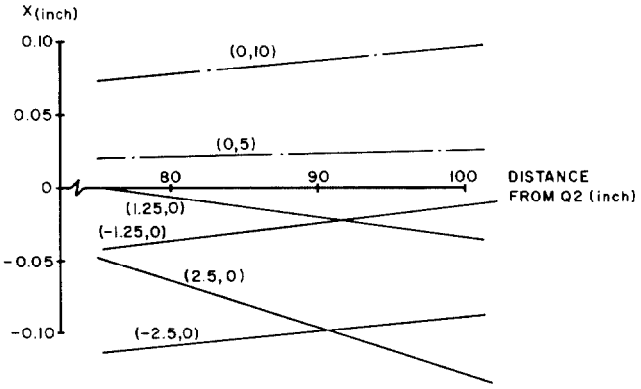

Fig. 5. A projection in the median plane in the region of S2 of the trajectories of 50 MeV protons traced through the analysis system of Figure 2, excluding the sextupoles, by the non-linear program Cartax. The rays originate from a point source on the optic axis at S1 with the initial divergence (x',y'), in milli-radians, shown.

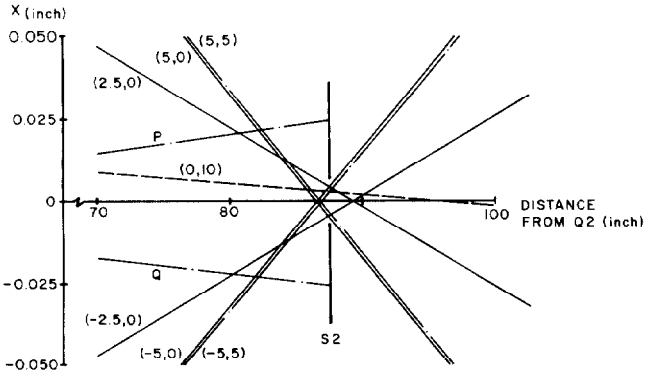

Fig. 6. An illustration of the effect of the sextupoles Sx1 and Sx2. A projection in the median plane at S2 of a similar set of rays as those shown in Figure 5, traced through the analysis system including sextupoles. P and Q are the paths of 49.99 MeV and 50.01 MeV protons initially moving along the optic axis.

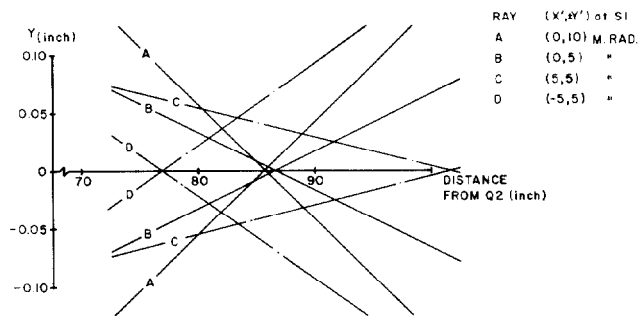

Fig. 7. A projection in the vertical plane of some of the rays of Figure 6.